Research on Trajectory Planning Method for Variable Sweep Back Aircraft with No Fly Zone Margin

Liang Qu [1, *], Peng Wang [1], and Hao He [1]

[1] College of Air and Space Science, National University of Defense Technology, Changsha, Hunan,410073.

* 1246254064@qq.com

Abstract. For a high-speed variable sweep aircraft, the variation characteristics of lift coefficient and drag coefficient with angle of attack were analyzed. Based on the analyzed aerodynamic characteristics, an aerodynamic parameter calculation model was established with Mach number, angle of attack, and deformation rate as independent variables. A no fly zone avoidance strategy with a no fly zone margin is proposed to address the issue of some inter point trajectories not meeting the constraints of the no fly zone when using the pseudospectral method for trajectory design. Its effectiveness is verified in cylindrical and elliptical no fly zones. The trajectory optimization design of the deformable aircraft was carried out with three different optimal objectives: maximum range, maximum final speed, and minimum flight time. The results of on-demand deformation rate and fixed deformation rate were compared and analyzed. The simulation results showed that the deformable aircraft had better flight ability under on-demand deformation rate. At the same time, the addition of sweep angle as the control variable increased the redundancy of control variables, Improved the anti saturation ability of the servo.

Keywords: Morphing vehicle; Pseudo-spectral method; No-fly zone margin; trajectory plannin g.

1. Introduction

Deformable aircraft refers to the aircraft that can actively change its aerodynamic shape according to different mission requirements and flight environment characteristics, generate different aerodynamic efficiency, better adapt to complex flight environment and perform flight tasks more optimally. Compared with traditional fixed-shape aircraft, deformed aircraft can increase the flight envelope range and flexibility, reduce unnecessary energy consumption at different flight stages, and improve the redundancy of the control system [1][2]. For high-speed aircraft, trajectory planning is an important part to explore and develop the performance of the aircraft [3]. Therefore, reasonable trajectory planning can make the deformed aircraft better play the advantages of the above-mentioned deformed aircraft and break through the performance limitations of the existing fixed-shape aircraft.

In terms of trajectory planning, considering the restriction of no-fly zone, literature [4] uses the Legendre polynomial root distribution characteristics to set waypoints near no-fly zone to increase the number of discrete points near no-fly zone and improve the accuracy of pseudo-spectral method to ensure that the restriction of no-fly zone is fully satisfied. In literature [5], the pseudo-spectrum method was used to optimize the trajectory of a two-stage telescopic wing variable shape glide vehicle, and its performance improvement compared with ordinary aircraft in different aspects was studied, including the ability to circumnavigate the no-fly zone. Literature [6] designed a certain rate of change of the heeling Angle to avoid the no-fly zone according to the constraints of quasi-balanced glide conditions. In reference [7], aiming at the no-fly zone problem, pseudo-spectral method is used for certain iteration to determine the "splicing points" around the no-fly zone, and the trajectory is segmented optimization to avoid the no-fly zone. In literature [8], energy is taken as an independent variable, the analytical formula of glide trajectory is derived, and the flip rule of heeling Angle is designed based on this analytical formula to successfully avoid the no-fly zone. The above methods can be roughly divided into two categories: one is based on the direct method algorithm to optimize the solution, in this kind of method, only the fuzzy selection

method of the waypoint or the specific strategy of avoiding the no-fly zone is given; Secondly, trajectory planning is carried out based on the derived analytic formula. In such methods, some methods only verify the effectiveness of the method for some time periods in the flight, without giving the whole trajectory. Some methods result in a larger error because of the analytical formula.

In view of the above problems and the possibility that the trajectories between the pseudo-spectral method may not meet the constraints of the no-fly zone, this paper proposes a method of "no-fly zone margin" based on the pseudo-spectral method, which can effectively avoid the no-fly zone, and verifies the effectiveness of the method in the case of cylindrical no-fly zone and elliptic cylindrical no-fly zone. The trajectory optimization results of variable sweep aircraft at maximum range, maximum final velocity and minimum flight time under demand deformation and fixed deformation rate are compared and analyzed, and the improvement of the performance of the aircraft in different aspects by introducing deformation is studied.

2. Reentry model Motion model and aerodynamic model

2.1 Equation of reentry motion

In the problem of reentry trajectory planning, we usually convert the motion of the reentry vehicle into the pole-changing coordinate system, which is to build a new equatorial arc with the starting point and the ending point. For the derivation of the model under the pole-changing coordinate system, see the reference [9]. In this way, the planned trajectory control quantity and state quantity display are more intuitive, and can solve the strange phenomenon of equations caused by the absolute latitude of 90° when the aircraft passes through the North and South Poles, simplifying the planning algorithm. Assuming that the Earth is a rotating homogeneous sphere, the motion equation of the general reentry vehicle can be obtained in the polar change coordinate system:

$$\begin{cases} \dfrac{\mathrm{d}r}{\mathrm{d}t} = v\sin\theta \\ \dfrac{\mathrm{d}\lambda}{\mathrm{d}t} = v\cos\theta\sin\psi/(r\cos\varphi) \\ \dfrac{\mathrm{d}\varphi}{\mathrm{d}t} = v\cos\theta\cos\psi/r \\ \dfrac{\mathrm{d}v}{\mathrm{d}t} = -D/m - g\sin\theta + \tilde{C}_v \\ \dfrac{\mathrm{d}\theta}{\mathrm{d}t} = [L\cos\sigma/m + (v^2/r - g)\cos\theta]/v + \tilde{C}_\theta + C_\theta \\ \dfrac{\mathrm{d}\psi}{\mathrm{d}t} = (L\sin\sigma/m\cos\theta + v^2\cos\theta\sin\psi\tan\varphi/r)/v + \tilde{C}_\psi + C_\psi \end{cases} \tag{1}$$

Where, r is the geocentric distance, λ is the longitude, φ is the dimension, v is the velocity of the aircraft with respect to the Earth, θ is the inclination Angle of local velocity, ψ is the track yaw Angle, and σ is the heeling Angle. $\tilde{C}_v$, $\tilde{C}_\theta$, $\tilde{C}_\psi$ is the implicated acceleration term; . C_θ , C_ψ Is Coriolis acceleration term, and its specific expression and related derivation are detailed in literature [9].

2.2 Aerodynamic characteristics analysis and aerodynamic modeling

Before establishing the aerodynamic calculation model, the aerodynamic data at different flight state points are analyzed, so that we can calculate and fit the aerodynamic parameters according to the obtained rules. Lift, drag coefficient and lift-drag ratio change with different flight status points as shown in FIG. 1-Fig. 4:

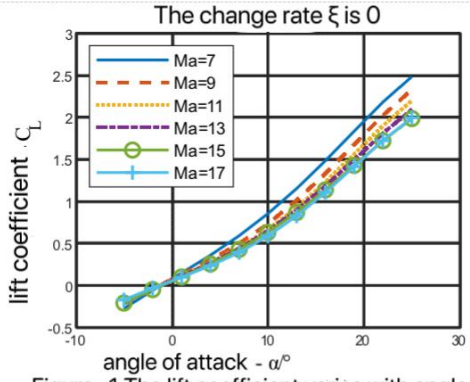

Figure -1 The lift coefficient varies with angle of attack and Ma when the change rate is 0.

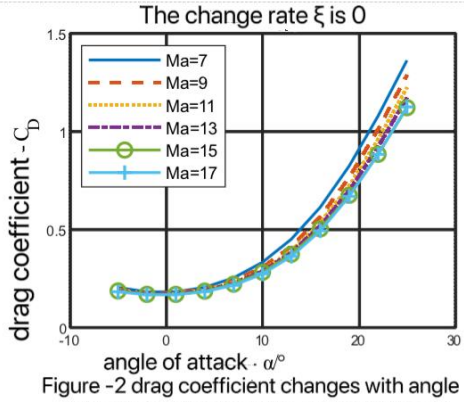

Figure -2 drag coefficient changes with angle of attack and Ma when the change rate is 0.

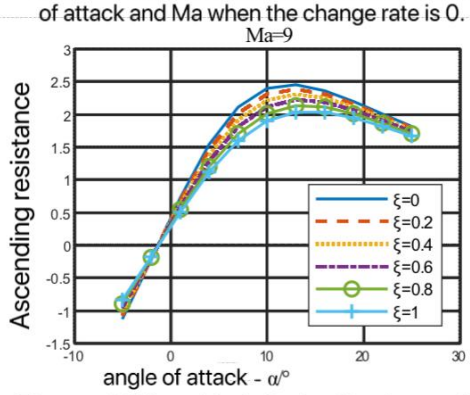

Figure -3 When Ma is 9, the lift-drag ratio changes with attack angle and change rate.

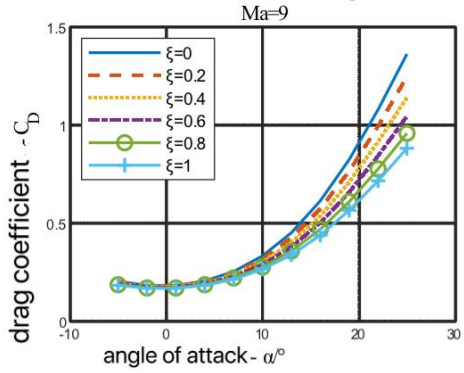

Figure-4 Variation of drag coefficient with angle of attack and deformation rate when Ma is 9.

As can be seen from FIG. 1, when the deformation rate is 0 and the velocity is low, the lift coefficient has an approximate linear relationship with the Angle of attack, but with the increase of the velocity, the quadratic correlation between the lift coefficient and the Angle of attack becomes stronger. The quadratic relationship between the resistance coefficient and the Angle of attack is obvious in Figure -2, and the same is true for other deformation rates, which will not be shown too much here. Based on the above analysis, lift and drag coefficients are synthesized in the following form:

$$\begin{cases} C_L = C_{L0}(Ma,\xi) + C_{L1}(Ma,\xi)\alpha + C_{L2}(Ma,\xi)\alpha^2 \\ C_D = C_{D0}(Ma,\xi) + C_{D1}(Ma,\xi)\alpha + C_{D2}(Ma,\xi)\alpha^2 \end{cases} \tag{2}$$

In addition, it can be seen from FIG. 3 that when Ma is 9, the lift-drag ratio decreases with the increase of deformation rate. It can be seen from FIG. 4 that when Ma=9, the drag coefficient decreases with the increase of the deformation rate, and the change law of the lift resistance ratio and drag coefficient above is also the same under other velocity states. It should be noted that the sweep Angle variation range of this aircraft is 45° ~ 75°, the corresponding deformation rate is 0 when the sweep Angle is 45°, and the corresponding deformation rate is 1 when the sweep Angle is 75°.

Lift and drag can be calculated as follows:

$$\begin{cases} L = 0.5\rho v^2 S C_L \\ D = 0.5\rho v^2 S C_D \end{cases} \tag{3}$$

Thus, the complete model of hypersonic variable sweep vehicle including motion model and aerodynamic model has been established.

3. Trajectory planning method with no-fly zone margin

3.1 Trajectory planning method design

Among the trajectory planning algorithms of many direct methods, the pseudo-spectral method takes the roots of orthogonal polynomials as discrete points, which is different from common equidistant discrete methods, and can obtain higher solution accuracy with fewer collocation points [10], and has been successfully applied in practical engineering [11][12]. In this paper, the pseudo-spectral method is used to plan the trajectory of the reentry section of a high speed variable sweep aircraft under two conditions of deformation on demand and constant deformation rate. However, when the pseudo-spectral method is used to design the no-fly zone avoidance trajectory, it can only ensure that the matching points strictly meet the constraints of the no-fly zone, and the trajectories between the matching points may cross the no-fly zone, as shown in Figure 5-7.

In view of the above problems, this paper proposes A new method to avoid the no-fly zone: the scope of the no-fly zone is reconstructed, that is, the radius (or long semi-axis and short semi-axis) are increased by 10%. As shown in Figure -8, the part between the red dotted line and the no-fly zone is called "no-fly zone margin". In this way, the trajectory between the matching points A and B can fully satisfy the constraints of the no-fly zone.

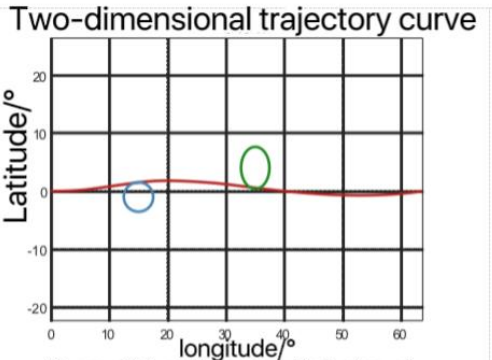

Figure -5 Two-dimensional trajectory of no-fly zone constraint being destroyed

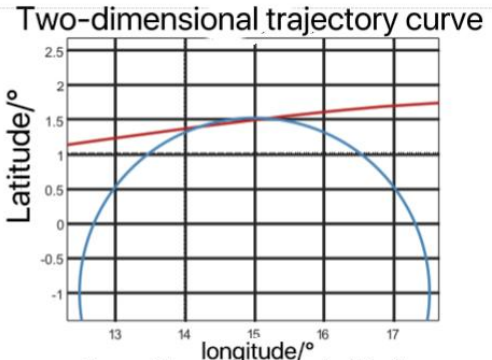

Figure -6 Local Enlargement of No-fly Zone Constraint 1 Damage

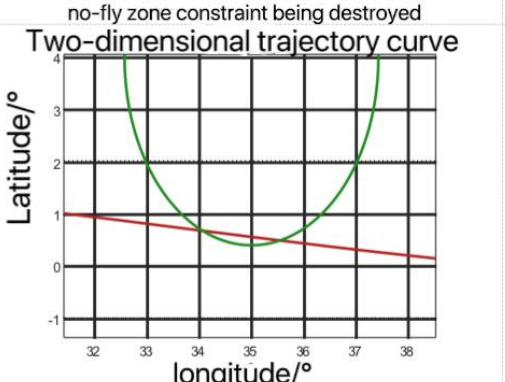

Figure -7 Partial enlarged view of no-fly zone constraint 2 being destroyed

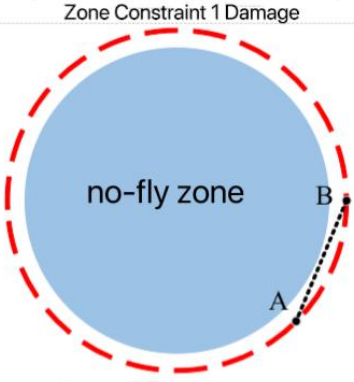

Figure -8 Schematic diagram of no-fly zone margin

3.2 Constraint Model

When using pseudo-spectral method for trajectory planning, it is usually necessary to consider several process constraints, such as heat flux, dynamic pressure and overload constraints, as shown below:

$$\begin{cases} \dot{Q} = k_q \rho^{0.5} v^{3.15} \le \dot{Q}_{\max} \\ q = 0.5 \rho v^2 \le q_{\max} \\ n = \sqrt{L^2 + D^2} \ / mg_0 \le n_{\max} \end{cases} \tag{4}$$

Where $\dot{Q}$, q, n respectively are heat flux, dynamic pressure, overload; ρ Is the atmospheric density; L and D are lift and drag forces respectively. In addition to the three process constraints, control amplitude and rate of change constraints should also be considered:

$$\begin{cases} \alpha \in [\alpha_{\min}, \alpha_{\max}], \dot{\alpha} \le \dot{\alpha}_{\max} \\ \sigma \in [\sigma_{\min}, \sigma_{\max}], \dot{\sigma} \le \dot{\sigma}_{\max} \\ \xi \in [\xi_{\min}, \xi_{\max}], \dot{\xi} \le \dot{\xi}_{\max} \end{cases} \tag{5}$$

α, σ, ξ respectively are Angle of attack, Angle of inclination and deformation rate; The differentials of the three represent the rate of change of the control quantity. In addition, this paper considers two kinds of no-fly zone constraints, cylinder and elliptic cylinder, and then the no-fly zone is modeled.

In the celestial northeast coordinate system with $(r_N, \lambda_N, \varphi_N)$ as the center $o - x_N y_N z_N$ on the Earth's surface, the no-fly zone of the elliptical body is expressed as:

$$\frac{y_N^2}{R_L} + \frac{z_N^2}{R_B} \ge 1 \tag{6}$$

Where R_L and R_B represent the length of the semi-major axis of the ellipse in the east direction and the north direction respectively. If the position of any point p on the Earth's surface is (r, λ, φ), then in the geocentric coordinate system, the coordinates of point p can be expressed as:

$$\begin{cases} x = r\cos\varphi\cos\lambda \\ y = r\cos\varphi\sin\lambda \\ z = r\sin\varphi \end{cases} \tag{7}$$

According to the conversion relationship (8) between the geocentric coordinate system and the celestial northeast coordinate system, after substituting (7) into (8) and then into (6), the no-fly zone constraint expressed by the geocentric longitude, latitude and altitude can be obtained. In equation (8), r_0 is the radius of the earth; A cylindrical no-fly zone is defined when R_L and R_B in (6) are equal.

$$\begin{bmatrix} x_N \\ y_N \\ z_N \end{bmatrix} = \begin{bmatrix} \cos\varphi_N\cos\lambda_N & \cos\varphi_N\sin\lambda_N & \sin\varphi_N \\ -\sin\lambda_N & \cos\lambda_N & 0 \\ -\sin\varphi_N\cos\lambda_N & -\sin\varphi_N\sin\lambda_N & \cos\varphi_N \end{bmatrix} \bullet \begin{bmatrix} x \\ y \\ z \end{bmatrix} - \begin{bmatrix} r_0 \\ 0 \\ 0 \end{bmatrix} \tag{8}$$

3.3 Simulation parameter Settings

Since the simulation is carried out under the polar change coordinate system, the starting point at any latitude and longitude is converted to the polar change coordinate system from 0°, and the track yaw Angle is started from 90°, so the initial state is not specially set for these three points in the following simulation. Table -1 sets the boundary values of state quantity and control quantity; Table -2 sets the boundary values of process constraints. Table -3 lists the locations and ranges of no-fly zones. The terminal constraints of speed and height in Table -1 have not been written out for the time being, and different Settings will be set according to different optimization objectives during simulation.

Table -1 Setting of boundary values of state quantity and control quantity

Quantity of state	v (m/s)	θ (°)	h (km)	Controlled quantity	α (°)	σ (°)	ξ
Starting point state	6500	-1	70	Starting point state	10	0	0.1
Upper limit of process	6500	+10	70	Upper limit of process	25	+90	1
Lower limit of process	1000	-10	25	Lower limit of process	2	-90	0
Terminal upper limit	——	+10	——	Terminal upper limit	25	+90	1

Terminal lower limit	——	-10	——	Terminal lower limit	2	-90	0

Table -2 Constraint boundary value Settings

Process constraint	$\dot{Q}$(kw/m^2)	q (kPa)	n	$\dot{\alpha}$ (°/s)	$\dot{\sigma}$ (°/s)	$\dot{\xi}$
Upper limit of process	3800	100	4	+10	+40	+0.2
Lower limit of process	0	0	0	-10	-40	-0.2

Table -3 No-fly zone parameter Settings

	Central longitude	Central latitude	Semi-major axis(km)	Short half shaft(km)	Height(km)
No-fly zone 1	15	-1	280	280	70
No-fly zone 2	35	4	400	270	70

4. Simulation results and analysis

4.1 Maximum range simulation results and analysis

When the maximum range simulation is carried out, the two cases of on-demand deformation and fixed deformation rate of 0.4 are compared. Set the upper limit of terminal speed to 3000m/s and the lower limit to 1000/s; The upper and lower limits of the terminal height are set at 25km; The terminal latitude is set to 0°, and the optimization target is the maximum longitude, that is, the maximum range. The simulation results are shown in Figure 9-16.

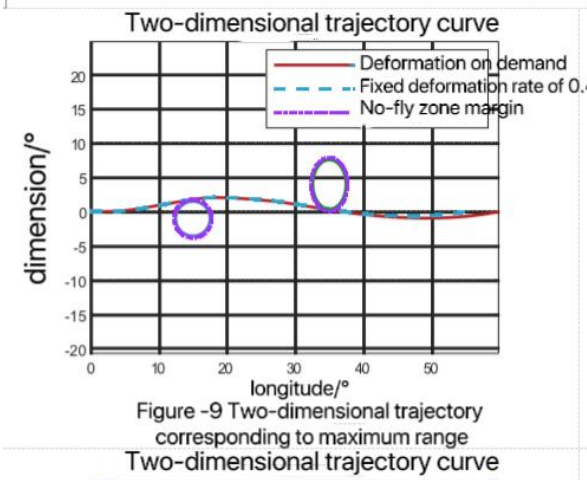

Figure -9 Two-dimensional trajectory corresponding to maximum range

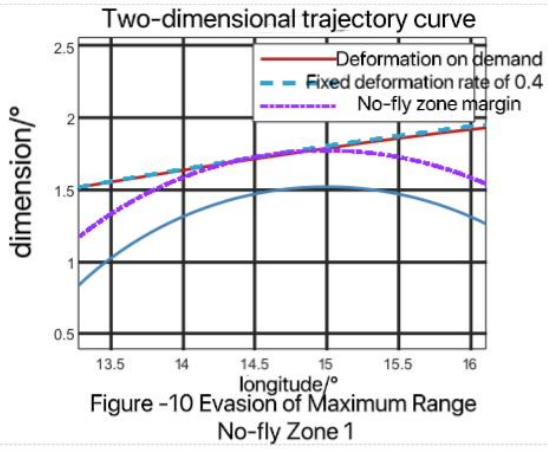

Figure -10 Evasion of Maximum Range No-fly Zone 1

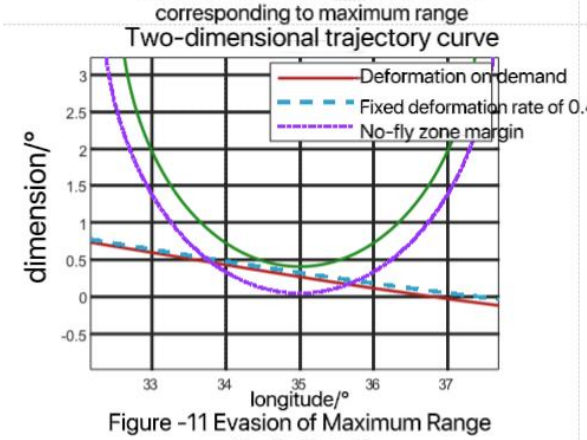

Figure -11 Evasion of Maximum Range No-fly Zone 2

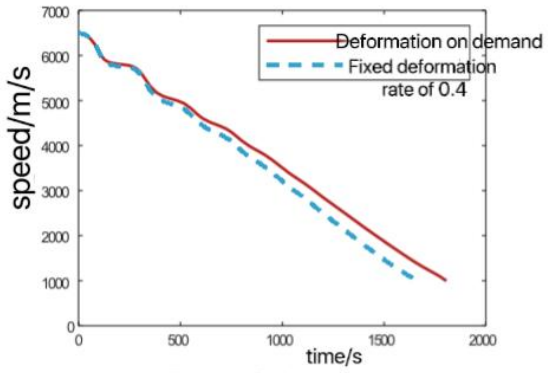

Figure -12 Maximum range speed change

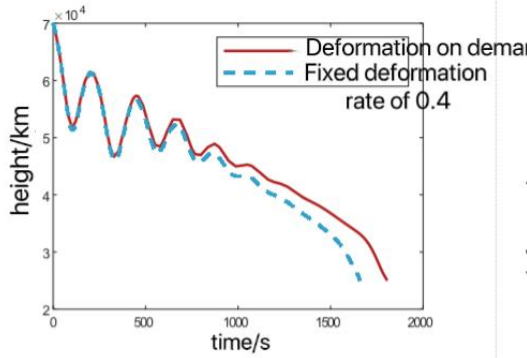

Figure -13 Maximum Range Height Change

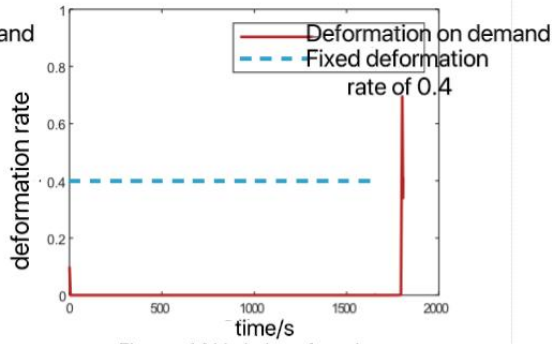

Figure -14 Variation of maximum range deformation rate

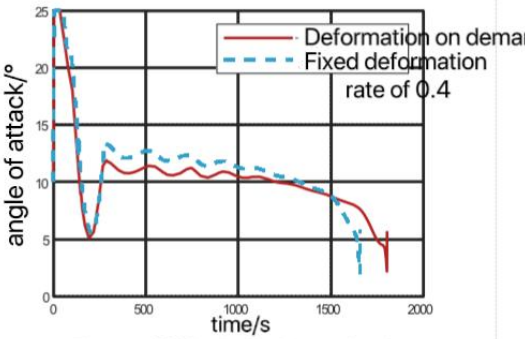

Figure -15 Maximum Range Angle of Attack Change

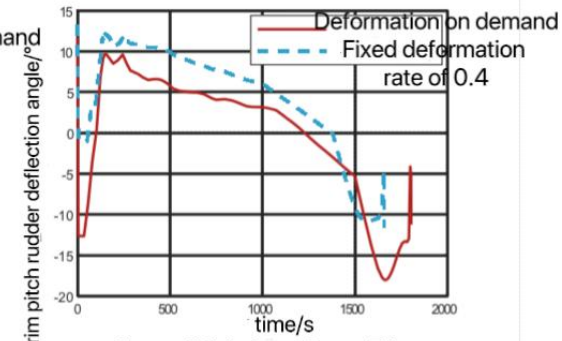

Figure -16 Maximum Range Trim Pitch Rudder Angle Change

As can be seen from Fig-9 to Fig-11, after the idea of "no-fly zone margin" is adopted in the two cases of on-demand deformation and fixed deformation rate, the two no-fly zones can be avoided better, and the terminal positions of the two are respectively (59.79,0) and (54.93,0), which indicates that the aircraft has a longer range under the condition of on-demand deformation. The range is 540.42km longer than that of the fixed deformation rate. At the same time, it can be seen from Fig-12 to Fig-13 that the aircraft can better maintain the altitude and speed in the reentry process to achieve a longer range under the condition of on-demand deformation. In Figure -14, the deformation rate under demand deformation is basically maintained at 0 throughout the whole process, which is because the lift-drag ratio decreases with the increase of the deformation rate, as can be seen from Figure -3. Therefore, in order to achieve the longest range, the aircraft under demand deformation is maintained at the deformation rate of 0 throughout the whole process to maintain the maximum lift-drag ratio to achieve the longest range. In Figure -15, the Angle of attack under demand deformation and fixed deformation rate is always maintained at about 11°, because the maximum lift-drag ratio of the Angle of attack is about 11°, which can be seen from Figure -3. Therefore, in order to achieve the longest range, the aircraft needs to maintain the Angle of attack near 11° in both cases. In Figure -15, the Angle of attack in the case of deformation on demand is smaller than that in the case of constant deformation for most of the time. As shown in Figure -16, the absolute value of trim pitch rudder yaw Angle under demand deformation is smaller than that of fixed deformation rate in most of the whole process, which indicates that the amplitude of attack Angle can be reduced by adjusting the deformation amount, and then the magnitude of pitch rudder yaw Angle can be reduced, the pressure of steering gear can be alleviated, and the risk of control failure can be reduced.

4.2 Maximum final speed simulation results and analysis

The two cases of demand deformation and fixed deformation rate of 0.4 are also compared. Set the upper limit of terminal speed to 6500m/s and the lower limit to 1000m/s; The upper limit of terminal height is 70km, the lower limit is 25km; The end point is set to be within the maximum

range of the two (50,0), and the optimization goal is the maximum final speed. The two can also avoid the no-fly zone well, and the simulation results are shown in Figure 17-24:

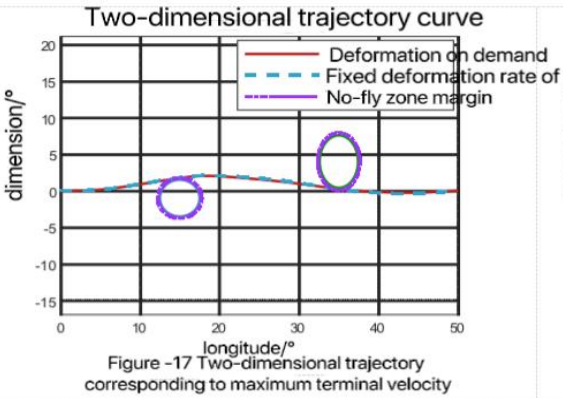

Figure -17 Two-dimensional trajectory corresponding to maximum terminal velocity

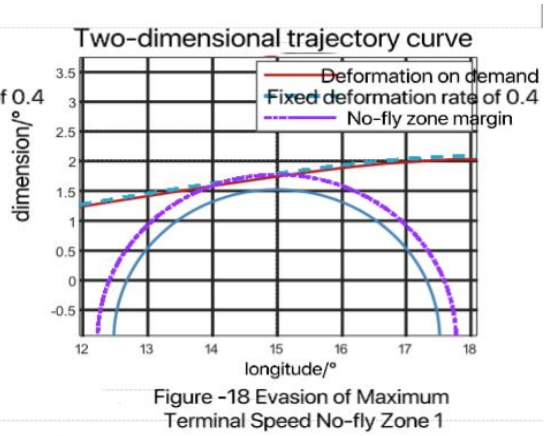

Figure -18 Evasion of Maximum Terminal Speed No-fly Zone 1

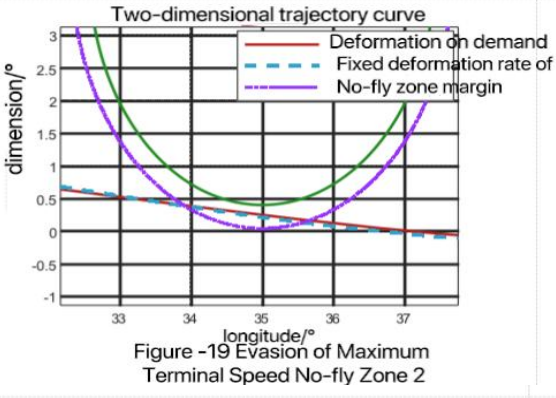

Figure -19 Evasion of Maximum Terminal Speed No-fly Zone 2

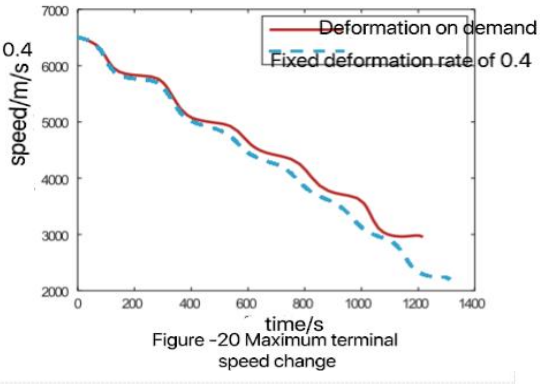

Figure -20 Maximum terminal speed change

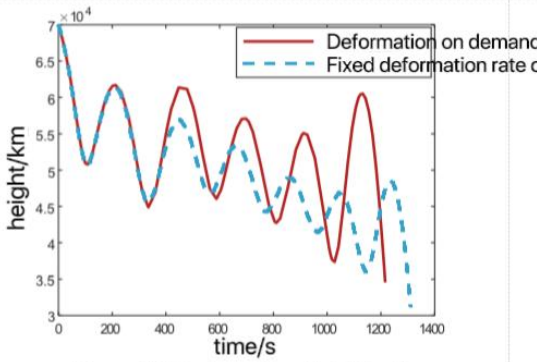

Figure -21 Maximum Terminal Velocity Height Change

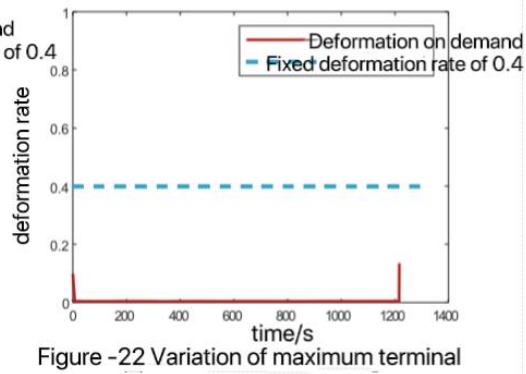

Figure -22 Variation of maximum terminal velocity deformation rate

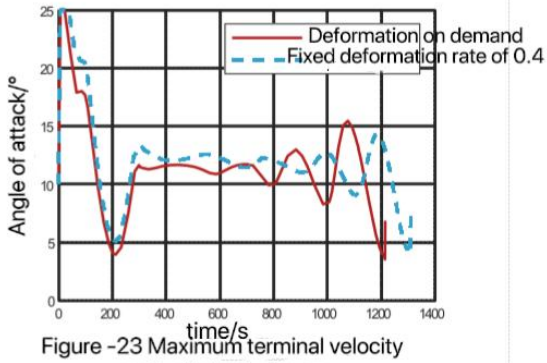

Figure -23 Maximum terminal velocity angle of attack change

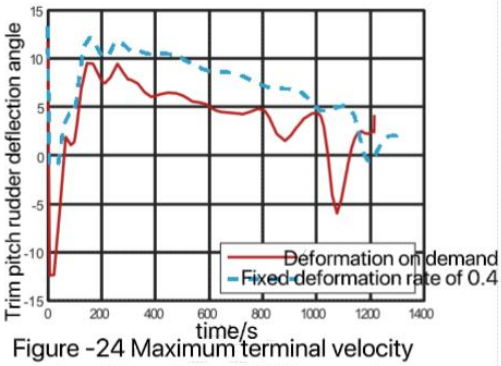

Figure -24 Maximum terminal velocity trim pitch rudder deflection angle

As shown in Figure -20, the terminal velocity in the case of on-demand deformation is 2952m/s, while that in the case of fixed deformation rate is 2209m/s, which is 743m/s less than that in the case of on-demand deformation, indicating that the aircraft has a higher final velocity under on-demand deformation. As can be seen from Figure -21, both of them have drastic changes in

height, and the height fluctuation in the case of on-demand deformation is greater than that in the case of fixed deformation rate. The movement time in the high-density sparse atmosphere is longer, and the speed loss caused by the resistance is smaller, so the final velocity can be obtained at last. This can also be seen from Figure -20. The time period in Figure -20 with slower speed reduction corresponds to the time period in Figure -21 with a higher altitude in the airspace. In Figure -23, the Angle of attack under demand deformation is smaller in most of the time than that under fixed deformation rate. In Figure -24, the absolute value of trim pitch rudder yaw Angle under demand deformation is also smaller in most of the time than that under fixed deformation rate. It also indicates that the amplitude of attack Angle can be reduced by adjusting the deformation amount, thus reducing the magnitude of pitch rudder yaw Angle and relieving the steering gear pressure. Reduce the risk of control failure.

4.3 Simulation results and analysis of minimum flight time

The simulation conditions of the minimum flight time are exactly the same as those of the maximum final speed, and the no-fly zone can also be well avoided. The simulation results are shown in Figure -25 to Figure -32:

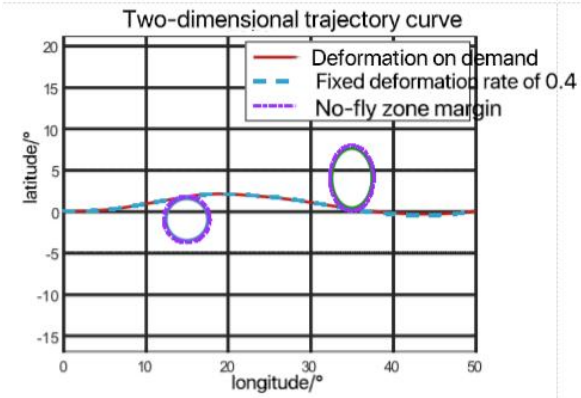

Figure -25 Two-dimensional trajectory corresponding to minimum flight time

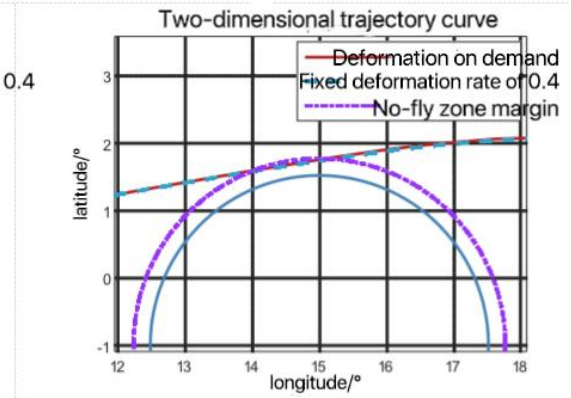

Figure -26 Evasion of Minimum Flight Time No-fly Zone 1

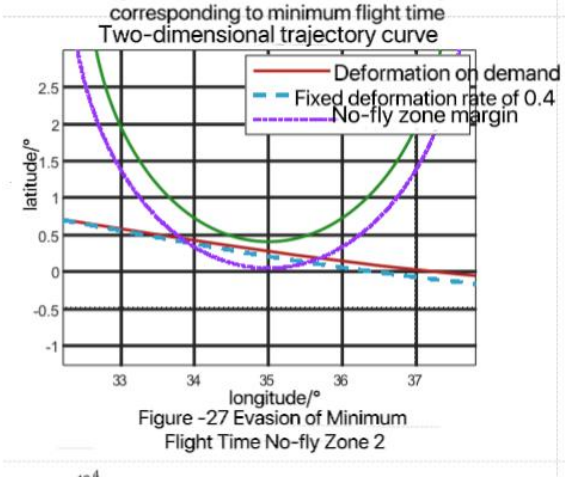

Figure -27 Evasion of Minimum Flight Time No-fly Zone 2

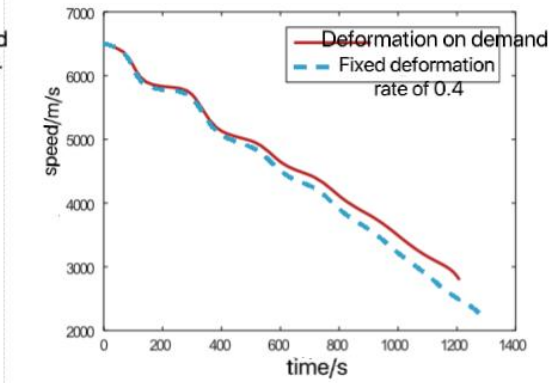

Figure -28 Minimum flight time speed change

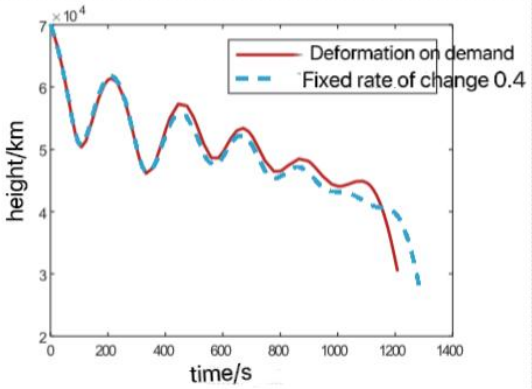

Figure -29 Minimum Flight Time Height Change

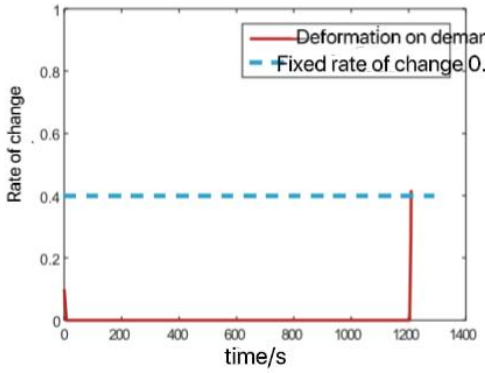

Figure -30 Variation of minimum flight time deformation rate

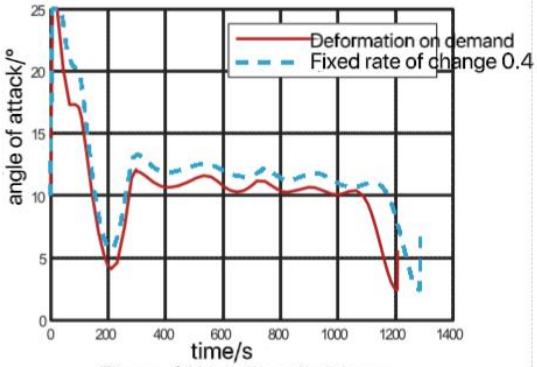

Figure -31 Variation of minimum flight time angle of attack

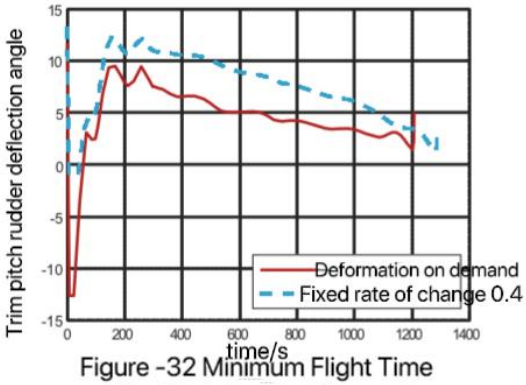

Figure -32 Minimum Flight Time Trim Pitch Rudder Changed

The fastest arrival time of on-demand deformation is 1208s, and the fastest arrival time of fixed deformation rate is 1287s, indicating that on-demand deformation has better rapid arrival ability than fixed deformation rate. In most of the time, the Angle of attack is also smaller than that in the case of fixed deformation rate, and the absolute value of trim pitch rudder deflection Angle is smaller than that in the case of fixed deformation rate, which also indicates that the introduction of deformation can alleviate the pressure of the steering gear and better avoid the risk of loss of control.

5. Conclusion

In this paper, the aerodynamic law of a variable sweep hypersonic vehicle is analyzed, and the aerodynamic model is established according to the aerodynamic law. In view of the situation that the restriction of no-fly zone may be broken between two matching points when using pseudo-spectral method, an idea of adding "no-fly zone margin" to avoid no-fly zone is proposed, and its effectiveness is verified by simulation in cylindrical no-fly zone and elliptic cylindrical no-fly zone. In addition, considering the influence of no-fly zone, the comparison simulation between the demand deformation and the fixed deformation rate is carried out. The three optimal objectives of the simulation are maximum range, maximum final velocity and minimum flight time. The results show that the performance of the deformable aircraft in these three aspects is better than that of the fixed deformation rate. The introduction of variable sweep as the control quantity can indeed improve the range, end strike ability and rapid arrival ability of the aircraft, and reduce the pressure of the control system.

Reference

[1] Peng Wang, Haolan Chen, Cunyu Bao, Guojian Tang. Review on modeling and control methods of deformable aircraft [J]. Journal of Astronautics,2022, vol. 43 (7): 853-865

[2] Xuhui ZHANG, Chunlei Xie, Sijia Liu, Ming Yan, Siyuan Xing. Analysis of development requirements and difficulties of intelligent deformable aircraft [J]. Acta Aeronautica et Astronautica Sinica,2023, vol. 44 (21): 8-34

[3] Xinle FENG. Research on trajectory optimization of Hypersonic vehicle based on Adaptive Pseudo-spectrum method [D]. University of Electronic Science and Technology of China,2021

[4] Yu Xie, Luhua Liu, Guojian Tang, Wei Zheng. Trajectory optimization of hypersonic glide vehicle under multiple constraints [J]. Journal of Astronautics,2011,(12): 2499-2504

[5] Tiebiao Chen, Min Gong, Hongbo WANG, Chenxi Wang, Zeyu XU. Trajectory optimization and performance analysis of deformable glide vehicle in near space [J]. Journal of Astronautics,2018, vol. 39 (9): 944-952

[6] Kenan Zhang, Hao Zhou, Wanchun Chen. Trajectory planning of hypersonic vehicle with multiple constraints and multiple maneuvering penetration modes [J]. Acta Ballistics Sinica,2012,(3): 85-90

[7] Changsheng Gao, Erkang Chen, Wuxing Jing. Maneuver avoidance trajectory optimization for hypersonic vehicle [J]. Journal of Harbin Institute of Technology,2017, vol. 49 (4): 16-21

[8] Yu, WB (Yu, Wenbin); Chen, WC (Chen, Wanchun); Jiang, ZG (Jiang, Zhiguo); Zhang, WQ (Zhang, Wanqing); Zhao, PL (Zhao, Penglei).Analytical entry guidance for coordinated flight with multiple no-fly-zone constraints.[J].Aerospace Science & Technology,2019,Vol.84: 273-290

[9] Xie,Y(Xie,Yu); Liu,LH(Liu,Luhua); Liu,J(Liu,Jun); Tang,GJ(Tang,Guojian); Zheng,W(Zheng,Wei).Rapid generation of entry trajectories with waypoint and no-fly zone constraints[J].ACTA ASTRONAUTICA,2012,Vol.77: 167-181

[10] Xixiang Yang, Huixin Yang, Peng Wang. Pseudo-spectrum method and its application in aircraft trajectory optimization design [J]. Journal of National University of Defense Technology,2015, 37 (4): 1-8

[11] Bollino, Kevin P. High-fidelity real-time trajectory optimization for reusable launch vehicles[D].Naval Postgraduate School,2018

[12] Bedrossian, Nazareth S, Bhatt, Sagar, Kang Wei, Ross, I. Michael.Zero-propellant maneuver guidance: rotating the International Space Station with computational dynamic optimization[J].IEEE Control Syst. Mag.,2009,Vol.29: 53-73.